1. Partial melting model and partition coefficients

The partial melting model is based on the batch melting equation (Shaw, 1970):

$$C^L = C^0 \times \frac{1}{D + F(1 - D)}$$

where C^L is the concentration of an element in the melt, C^0 is the concentration of the element in the source rock (protolith), D is the average bulk partition coefficient for the residual minerals, and F is the weight fraction of melt produced during partial melting (degree of partial melting). The average bulk partition coefficient (D) is determined using the following equation:

$$D = \sum_{i=1}^{n} D_i \times X_i$$

where D_i is the partition coefficient of an element between the melt and an individual residual mineral (i), X_i is the weight percentage of this residual mineral (i) in the total resitite, and n is the total number of minerals involved in partial melting. The partial melting modeling results are shown in Table S3.

The mineral-melt partition coefficients (except for that for garnet) used in this study were adopted from Simons et al. (2017) who derived the partition coefficients for W and Sn between granitic melt and a series of minerals by phenocryst/matrix measurements of Sn-W-related granites of the Cornbian Batholith in southwestern England. In general, mineral-melt partition coefficients are influenced mainly by composition of the melt, and to a lesser degree by temperature, pressure, and oxygen fugacity (Candela and Bouton, 1990; Icenhower and London, 1995, 1996; Adam and Green, 2007; Simons et al., 2017). We note that the melt composition derived from a low-degree partial melting is similar to that after a high-degree fractional crystallization (Icenhower and London, 1995, 1996; Patiño Douce and Harris, 1998; King et al., 2011; Taylor et al., 2014; Xia et al., 2019). Other conditions for the crystallization of granitic melt are also broadly similar to those for partial melting of metasedimentary rocks (Icenhower and London, 1995, 1996; Patiño Douce and Harris, 1998; Romer and Kroner, 2016). Therefore, the partition coefficients for granites of Simons et al. (2017) are applicable to partial melting (Icenhower and London, 1995; Simons et al., 2017).

The bulk partition coefficients (except for that for garnet) from Simons et al. (2017) may have been affected by the proportions of biotite and muscovite in the granites, because previous studies have suggested that W and Sn are hosted mainly in micas (Romer and Kroner, 2016; Simons et al., 2017; Wolf et al., 2018; Yuan et al., 2019). To assess the uncertainties introduced by the partition coefficients (D), we recalculated the partition coefficients by intentionally adding or removing 5 wt% biotite and/or muscovite. The amount, 5 wt%, was used because Simons et al. (2017) suggested that the modal percentages of muscovite and biotite are less than 10%. The results are listed in the table below which shows that the D values for biotite vary between -2% and +13% relative to the original data, and the D values for muscovite vary between -35% and +115% relative to the original data. The variation in the D values for biotite is relatively small and has limited influence on the results of the modeling (Fig. 3). The variation in D values for muscovite is larger. However, this does not influence the overall conclusion, because all the muscovite is consumed before the melt is extracted (Fig. 3). In other words, this study focused on the W and Sn concentrations in melt after muscovite was exhausted during partial melting. Thus, the errors in the

partition coefficients of W and Sn introduced by the biotite and muscovite proportions in the granites considered in Simons et al. (2017) have a minimal effect on the results of this study. The propagated errors for the W and Sn concentrations in the melt during partial melting are shown as error envelopes in Figure 3.

Mineral-melt Partition coefficients	Original data from Simons et al. (2017)		Data recalculated by removing 5 wt% of the mineral		Data recalculated by adding 5 wt% of the mineral	
	Biotite	Muscovite	Biotite	Muscovite	Biotite	Muscovite
Sn	2.32	4.14	2.6 (+13%)*	5.2 (+26%)	2.1 (-10%)	3.4 (-17%)
W	0.4	10.71	0.41 (+2%)	23.1 (+115%)	0.39 (-2%)	7.0 (-35%)

*The numbers in parentheses show the variation of *D* values relative to the original data. These numbers were calculated using the equation: (B-A)/A×100, where A is the original *D* value and B is the new *D* value.

To our knowledge, coefficients have not been reported for the partitioning of W, Sn and Ta between garnet and granitic melt during partial melting. In this study, we employed garnet-melt partition coefficients for W, Sn and Ta that we extracted from the results of analyses of garnet-bearing migmatites reported in Xia et a. (2019). The migmatites are from the Linzhi complex in the southeastern Lhasa terrane, Himalayan orogen (Xia et al., 2019). Partial melting occurred in the migmatites, producing a K-feldspar-bearing leucocratic vein, representing the melt formed by mica-dehydration melting, and leaving behind garnet of peritectic origin in the biotite gneiss (restite) (Xia et al., 2019). Phase equilibrium calculations, mineral assemblages, and garnet isopleths indicate that the peak anatectic conditions were 760-800 °C and 9-10.5 kbar (Xia et al., 2019). The melting conditions and the nature of melting (biotite dehydration) of these samples are similar to those of the partial melting model presented in this study. Therefore, we conclude that the garnet-melt partition coefficients obtained from these samples are applicable to this partial melting model. We calculated the garnet-melt partition coefficients for W, Sn, and Ta by combining the composition of the peritectic garnet (sample number: 12LS104) from Xia et al. (2019) with the composition of the leucocratic vein (sample number: 12LS104, which was kindly provided by Qiongxia Xia and is the sample referred to in Xia et al. 2019) from this study.

The analytical method used to determine the trace element content of the leucocratic vein and the analytical results are reported below. The trace element analyses were performed by Guizhou Tongwei Analytical Technology Co., Ltd. on a Thermal Fisher iCAP RQ ICP-MS equipped with a Cetac ASX-560 AutoSampler. Approximately 50 mg of rock powder was dissolved in a Teflon bomb with a doubly distilled concentrated HNO_3-HF (1 : 4) mixture. The dissolution occurred in an oven at 185°C for 3 days. The solutions were then dried to evaporate the HF. The sample residues were re-dissolved with doubly distilled concentrated HNO_3 followed by a 1:1 HNO_3 treament and dried again. The samples were then dissolved in a 3ml 2N HNO_3 stock solution. Finally, the solutions were diluted 4000 times with 2 percent HNO_3 and 9ppb ^{61}Ni, and 6ppb Rh, In and Re were added as internal spikes. The USGS standard, W-2a, was used as the reference standard and crossed checked with BHVO-2 and other reference materials. The instrument drift mass bios was corrected with internal spikes and external monitors. The ICP-MS procedure for trace element analysis followed the protocol of Eggins et al. (1997) with modifications described in Kamber et al. (2003), Li et al. (2005), and Li et al. (2019).

	Sn (ppm)	W (ppm)	Ta (ppm)
The composition of the leucocratic vein from this study	1.07	0.329	0.423
The composition of the peritectic garnet from Xia et al. (2019)	0.183	0.012	0.003
Partition coefficient	0.171	0.036	0.007

2. Fractional crystallization model

The fractional crystallization model was based on the Raleigh fractionation equation (Shaw, 1970):

$$C^L = C^0 \times F^{D-1}$$

where C^L is the concentration of an element in the melt, C^0 is its concentration in the initial melt, D is the bulk partition coefficient for the fractionating minerals, and F is the weight fraction of melt remaining in the system. The bulk partition coefficient was calculated in the same way as in the section above.

The minerals crystallized were assumed to be quartz, K-feldspar, plagioclase, biotite, and muscovite, which are common minerals in W- or Sn-related granites (Lehmann, 1990; Ballouard et al., 2016; Simons et al., 2017; and references in Table S1). Since the mineral-melt partition coefficients for quartz and K-feldspar are small (KD < 0.05, Table S2), the partitioning of W and Sn during fractional crystallization is mainly controlled by the proportions of plagioclase, biotite, and muscovite. The W- and Sn-related granites compiled in this study (references in Table S1) contain 10-25 wt% plagioclase, 5-10 wt% biotite and 3-5 wt% muscovite. These mineral propotions were used to estimate the whole-rock partition coefficients for W and Sn and were then used in the Rayleigh fractional crystallization model. For the purpose of sensitivity testing, the proportions of crystallized minerals were assumed to be in a range rather than to have a specific value. The results (Fig. 4) show that the variations in the proportions of minerals crystallized in the aforementioned ranges have limited influence on the modeling results, i.e., the melt generated at low-temperature muscovite-dehydration melting facilitates the enrichment of W in the melt and subsequent W mineralization, whereas the melt generated at high-temperature biotite-dehydration melting favors enrichment of Sn in the melt and subsequent Sn mineralization.

Redistribution of the elements between melt and restite after the melt had been extracted from the source was not considered in the fractionation model. This is because restite is rare in Sn-related granites, (Lehmann, 1990; Yuan et al., 2019; and references in Table S1). The rare occurrence of resitite in Sn-related granite might reflect the relatively high melting temperature (>750 °C), as the restite models typically apply to to melt generated at < 750 °C (Chappell et al., 2000; Stevens et al., 2007). In addition, the restite model does not explain the variation of geochemical composition in Sn granite suites (Lehmann, 1990) and the differences in whole-rock Sr-Nd and zircon Hf-O isotopic compositions between “mafic inclusions” and the host granites (Yuan et al., 2019 and references therein). To our knowledge, there is no documentation of restites in the W-related granites compiled in this study. Thus, restites, if they exist, are likely to be present in small volumes and therefore are unlikely to affect the behavior of W during magma fractionation. Furthermore, according to Chappell et al. (1987), the term restite in S-type granite refers predominantly to xenoliths of refractory fragments from the source (cordierite and, less commonly,

almandine garnet) and xenocrysts like calcic plagioclase relict cores, sillimanite, and inherent zircon. Since W is highly incompatible in these minerals (Table S2), the impact of restite should have a negligible influence on the behavior of W during fractional crystallization.

3. Explanation of supplementary Figures.

Supplementary Figures 1, 2 and 3 illustrate the zircon-saturation temperatures (T_{Zr}; Fig. S1), whole-rock W and Sn concentrations (Fig. S2), and the whole-rock Fe_2O_3/FeO ratios (Fig. S3) as functions of fractionation indices for W- or Sn-related granites in the W-Sn metallogenic belts compiled in Figure 1.

We used TiO_2, Nb/Ta, Zr/Hf, and Rb/Sr as the fractionation indices. Titanium is very insoluble in aqueous fluids and thus is extremely immobile during hydrothermal alteration of granite (Lehmann, 2020). During fractional crystallization of granitic magmas, Ti is moderately compatible in biotite and other early crystallizing Ti-bearing minerals, leading to its progressive depletion in the melt as fractionation proceeds (Lehamnn, 1990, 2020). Therefore, a trend of decreasing Ti concentration in a granite is an indication of fractional crystallization (Lehmann, 1990, 2020). The solubility of Nb, Ta, Zr and Hf in aqueous are also very low (Chevychelov et al., 2005; Borodulin et al., 2009; Migdisov et al., 2011; Timofeev et al., 2015, 2017) and they are almost invariably not affected by hydrothermal alteration. Furthermore, Nb and Ta, as well as Zr and Hf are considered to be "geochemical twins" because of their similar charges and ionic radii (Goldschmidt, 1937; Ballouard et al., 2016). However, the Nb/Ta and Zr/Hf ratios in granite will decrease in response to the fractionation of micas and zircon, respectively (Raimbault et al., 1995; Linnen and Keppler, 1997, 2002; Claiborne et al., 2006; Stepanov et al., 2014). Therefore, the Nb/Ta and Zr/Hf ratios in granite can also be used as indices of the degree of fractional crystallization (Ballouard et al., 2016; Yuan et al., 2019). The whole-rock Rb/Sr ratio is used as fractionation index, because of the preferential incorporation of Rb in late-crystalized K-feldspar and Sr in early plagioclase (Lehmann, 1990). For each ore-related granitic intrusion, we used several fractionation indices in parellel. The figures for each metallogenic belt were assembled in a single page.

In all the figures, the blue circles refer to W-related granites and orange diamonds refer to Sn-related granites. If different granite phases could be identified (e.g., granites related to the Shizhuyuan Sn-W deposit and Xihuashan W deposit in the Nanling region), different colors were used to distinguish early and late phases.

In Figure S1, the compiled data shows trends of decreasing zircon-saturation temperature (T_{Zr}) with increasing degree of fractional crystallization (gray arrows). Therefore, we used the least-evolved endmembers in individual intrusions to determine the melting temperatures of the metasedimentary rocks that produced the granitic magmas. The rarity of inherited zircon grains in high-temperature Sn-related magmas (Yuan et al., 2019 and references in Table S1) is evidence that zircon was initially undersaturated, which means that T_{Zr} provides a minimimum estimate of the temperature of melting (Miller et al., 2003). In contrast, the abundance of inherited zircon in low-temperature W-related granite artificially increases the Zr content of the bulk melt leading to overestimated temperatures. Thus, the difference in the initial magma temperatures estimated for W- and Sn-related granites might be even greater than presented in Figure 2.

In Figure S2, for most granites, both the whole-rock W and Sn concentrations increase with the degree of fractional crystallization, indicating that magma evolution did not lead to the depletion of W or Sn or the decoupling of W and Sn mineralization. In Figure S3, The Fe_2O_3/FeO ratios are largely independent of the degree of fractional crystallization, indicating that the redox states of these granites were not influenced by magma evolution but were likely inherited from the source regions.

References

Adam, J., and Green, T., 2006, Trace element partitioning between mica- and amphibolebearing garnet lherzolite and hydrous basanitic melt 1: experimental results and the investigation of controls on partitioning behaviour: Contributions to Mineralogy and Petrology, v.152, p. 1–17.

Ballouard, C., Pojol, M., Boulvais, P., Branquet, Y., Tartese, R., and Vigneresse, J., 2016, Nb-Ta fractionation in peraluminous granites: A marker of the magmatic-hydrothermal transition: Geology, v. 44, p. 231-234

Blevin, P.L., and Chappell, B.W., 1992, The role of magma sources, oxidation states and fractionation in determining the granite metallogeny of eastern Australia: Earth and Environmental Science Transactions of the Royal Society of Edinburgh, v. 83, p. 305-316

Blevin, P.L., and Chappell, B.W., 1995, Chemistry, origin, and evolution of mineralized granites in the Lachlan Fold Belt, Australia: the metallogeny of I- and S-type granites: Economic Geology, v. 90, p. 1604-1619, https://doi.org/10.2113/gsecongeo.90.6.1604

Borodulin, G.P., Chevychelov, V.Y., and Zaraysky, G.P., 2009, Experimental study of partitioning of tantalum, niobium, manganese, and fluorine between aqueous fluoride fluid and granitic and alkaline melts: Geochemistry, v. 427, p. 233-238.

Candela, P.A., and Bouton, S.L., 1990, The influence of oxygen fugacity on tungsten and molybdenum partitioning between silicate melts and ilmenite: Economic Geology, v. 85, p. 633-640.

Chappell, B.W., White, A.J.R., and Wyborn, D., 1987, The importance of residual source material (restite) in granite petrogenesis: Journal of Petrology, v. 28, p. 1111-1138.

Chappell, B.W., White, A.J.R., Williams, I.S., Wyborn, D., and Wyborn, L.A.I., 2000, Lachlan Fold Belt granites revisited: High- and low-temperature granites and their implications: Australian Journal of Earth Sciences, v. 47, p. 123–138.

Chevychelov, V.Y., Zaraisky, G.P., Borisovskii, S.E., and Borkov, D.A., 2005, Effect of melt composition and temperature on the partitioning of Ta, Nb, Mn, and F between granitic (Alkaline) melt and fluorine-bearing aqueous fluid: fractionation of Ta and Nb and conditions of ore formation in rare-metal granites: Petrology, v. 13, p. 305-321.

Claiborne, L.L., Miller, C.F., Walker, B.A., Wooden, J.L., Mazdab, F.K., and Bea, F., 2006, Tracking magmatic processes through Zr/Hf ratios in rocks and Hf and Ti zoning in zircons: An example from the Spirit Mountain batholith, Nevada: Mineralogical Magazine, v. 70, p. 517-543.

Eggins, S.M., Woodhead, J.D., Kinsley, L.P.J., Mortimer, G.E., Sylvester, P., McCulloch, M.T., Hergt, J.M., and Handler, M.R., 1997, A simple method for the precise determination of ≥40 trace elements in geological samples by ICPMS using enriched isotope internal standardisation: Chemical Geology, v. 134, p. 311–326, http://dx.doi.org/10.1016/S0009-2541(96)00100-3

Goldschmidt, V.M., 1937, The principles of distribution of chemical elements in minerals and rocks: The seventh Hugo Müller Lecture delivered before the Chemical Society on March 17th, 1937: Journal of the Chemical Society, v. 1937, p. 655-673.

Guo, L., Zhang, H.F., Harris, N., Luo, B.J., Zhang, W., and Xu, W.C., 2019, Tectonic erosion and crustal relamination during the India-Asian continental collision: Insights from Eocene magmatism in the southeastern Gangdese belt: Lithos, v. 346-347, p. 105161.

Icenhower, J., and London, D., 1995. An experimental study of element partitioning among biotite, muscovite, and coexisting peraluminous silicic melt at 200 MPa (H2O): American Geologist, v. 80, p. 1229-1251.

Icenhower, J., and London, D., 1996. Experimental partitioning of Rb, Cs, Sr and Ba between alkali feldspar and peraluminous melt: American Minealogist, v. 81, p. 719-734.

Kamber, B.S., Greig, A., Schoenberg, R., and Collerson, K.D., 2003, A refined solution to Earth's hidden niobium: implications for evolution of continental crust and mode of core formation: Precambrian Research, v. 126, p. 289–308, http://dx.doi.org/10.1016/S0301-9268(03)00100-1

King, J., Harris, N., Argles, T., Parrish, R. & Zhang, H. (2011). Contribution of crustal anatexis to the tectonic evolution of Indian crust beneath southern Tibet. Geological Society of America Bulletin, v. 123, p. 218–239.

Lehmann, B., 1990, Metallogeny of tin: Berlin, Springer.

Lehmann, B., 2020, Formation of tin ore deposits: A reassessment. Lithos, 105756.

Li, B.P., Greig, A., Zhao, J.X., Collerson, K.D., Quan, K.S., Meng, Y.H., and Ma, Z.L., 2005, ICP-MS trace element analysis of Song dynasty porcelains from Ding, Jiexiu and Guantai kilns, north China: Journal of Archaeological Science, v. 32, p. 251–259, http://dx.doi.org/10.1016/j.jas.2004.09.004

Li, H.Y., Taylor, R.N., Prytulak, J., Kirchenbaur, M., Shervais, M.J., Ryan, J.G., Godard, M., Reagan, M.K., Pearce, J.A., 2019. Radiogenic isotopes document the start of subduction in the Western Pacific. Earth and Planetary Science Letters, v. 518, p. 197-210.

Linnen, R.L., and Keppler, H., 1997, Columbite solubility in granitic melts: Consequences for the enrichment and fractionation of Nb and Ta in the Earth's crust: Contributions to Mineralogy and Petrology, v. 128, p. 213-227.

Linnen, R.L., and Keppler, H., 2002, Melt composition control of Zr/Hf fractionation in magmatic processes: Geochimica et Cosmochimica Acta, v. 66, p. 3293-3301.

Mao, J.W., Ouyang, H.G., Song, S.W., Santosh, M., Yuan, S.D., Zhou, Z.H., Zheng, W., liu, H., Liu, P., Cheng, Y.B., and Chen, M.H., 2019, Geology and metallogeny of tungsten and tin deposits in China: Economic Geology, v. 22, p. 411-482.

Migdisov, A.A., Williams-Jones, A.E., Hinsberg, V., Salvi, S., 2011. An experimental study of the solubility of baddeleyite (ZrO_2) in fluoride-bearing solutions at elevated temperature: Geochimica et Cosmochimica Acta, v. 75, p. 7426-7434.

Miller, C.F., McDowell, S.M., and Mapes, R.W., 2003, Hot and cold granites? Implications of zircon saturation temperatures and preservation of inheritance: Geology, v. 31, p. 529-532.

Patino Douce, A.E., and Harris, N., 1998, Experimental constraints on Himalayan anatexis: Journal of Petrology, v. 39, p. 689-710.

Patiño Douce, A.E., and Harris, N., 1998, Experimental constraints on Himalayan anatexis: Journal of Petrology, v. 39, p. 689-710.

Raimbault, L., Cuney, M., Azencott, C., Duthou, J.-L., and Joron, J.L., 1995, Geochemical evidence for a multistage magmatic genesis of Ta-Sn-Li mineralization in the granite at Beauvoir, French Massif Central: Economic Geology and the Bulletin of the Society of Economic Geologists, v. 90, p. 548-576.

Romer, R.L., and Kroner, U., 2016, Phanerozoic tin and tungsten mineralization-tectonic controls on the distribution of enriched protoliths and heat sources for crustal melting: Gondwana Research, v. 31, p. 60-95, http://dx.doi.org/10.1016/j.gr.2015.11.002

Shaw, D.M., 1970. Trace element fractionation during anatexis. Geochimica et Cosmochimica Acta, v. 34, p. 237–243.

Simons, B., Andersen, J.C.Ø., Shail, R.K., and Jenner, F.E., 2017, Fractionation of Li, Be, Ga, Nb, Ta, In, Sn, Sb, W and Bi in the peraluminous Early Permian Variscan granites of the Cornubian batholith: Precursor processes to magmatic-hydrothermal mineralization: Lithos, v. 278, p. 491–512.

Stepanov, A., Mavrogenes, J.A., Meffre, S., and Davidson, P., 2014, The key role of mica during igneous concentration of tantalum: Contributions to Mineralogy and Petrology, v. 167, p. 1009-1016.

Taylor, J., Nicoli, G., Stevens, G., Frei, D. & Moyen, J. F. (2014). The processes that control leucosome compositions in metasedimentary granulites: Perspectives from the Southern Marginal Zone migmatites, Limpopo Belt, South Africa. Journal of Metamorphic Geology, v. 32, p. 713–742.

Timofeev, A., Migdisov, A.A., and Williams-Jone, A.E., 2015. An experimental study of the solubility and speciation of niobium in fluoride-bearing aqueous solutions at elevated temperature: Geochimica et Cosmochimica Acta, v. 158, p. 103-111.

Timofeev, A., Migdisov, A.A., and Williams-Jone, A.E., 2017. An experimental study of the solubility and speciation of tantalum in fluoride-bearing aqueous solutions at elevated temperature. Geochimica et Cosmochimica Acta, v. 197, p. 294-304.

Xia, Q.X., Gao, P., Yang, G., Zheng, Y.F., Zhao, Z.F., Li, W.C., and Luo, X., 2019, The origin of garnets in anatectic rocks from the eastern Himalayan syntaxis, southeastern Tibet: constraints from major and trace element zoning and phase equilibrium relationships. Journal of Petrology, v. 60, p. 2241-2280.

Yuan, S.D., Williams-Jones, A.E., Romer, R.L., Zhao, P.L., and Mao, J.W., 2019, Protolith-related thermal controls on the decoupling of Sn and W in Sn-W metallogenic province: insights from the Nanling region, China: Economic Geology, v. 114, p. 1005-1012.

Zhang, Z.M., Dong, X., Xiang, H., Liou, J.G., and Santosh, M., 2013, Building of the deep Gangdese arc, South Tibet: Paleocene plutonism and granulite-facies metamorphism: Journal of Petrology, v. 54, p. 2547-2580.

Table S1. Bulk compositions of W- and Sn-related granites in the Nanling W-Sn region (1A), the Jiangnan W belt (1B), the Southeast Asian Sn belt (1C), the Youjiang Sn belt (1D), the QQK W-Sn belt (1E), the Cornwall Sn region (1F), and the Bolivian Sn belt (1G).

Table S2. Mineral-melt partition coefficients used to model partial melting.

Table S3. Results of the modeling of mineral proportions and W and Sn concentration in melts and minerals during partial melting at T = 650-1000 ℃ and P = 0.5, 0.7 and 0.9 GPa.

Figure S1. Zircon-saturation temperature (T_{Zr}) as a function of the fractionation indices (Nb/Ta, Zr/Hf, Rb/Sr, and TiO_2) for W- or Sn-related granites in the major W-Sn metallogenic belts shown in Figure 1. Orange diamonds refer to Sn-related granites and blue circles refer to W-related granites. For individual intrusions, the grey arrows show the trend of decreasing magma temperature with increasing degree of fractional crystallization. Therefore, the least-evolved samples for individual intrusions were considered to best represent the melting temperature for the granite. The data are from Table S1.

Figure S2. Whole-rock W or Sn concentrations as a function of the fractionation index (whole-rock TiO_2 concentration) for W- or Sn-related granites in the W-Sn metallogenic belts shown in Figure 1. For most granites, both the W and Sn concentration increase with the degree of fractional crystallization, indicating that magma evolution did not lead to the depletion of the ore metal (e.g. W or Sn) and, thus, the decoupled behavior of W and Sn mineralization. The data are from Table S1.

Figure S3. Whole-rock Fe_2O_3/FeO ratios as a function of fractionation index (whole-rock TiO_2 concentration) for W- and Sn-related granites in the W-Sn metallogenic belts shown in Figure 1. The Fe_2O_3/FeO ratios are largely independent of the degree of fractional crystallization, indicating that the redox state of the granite was inherited from the source region. The data are from Table S1.

Figure S4. Results of the modeling of partial melting for pressures of 0.7 and 0.9 GPa. Figures A1 and B1 show the modal proportions of the phases as a function of temperature during partial melting of an average metapelite (White et al., 2007) and Figures A4 and B4 show the proportions after extraction of 10 wt% of the melt (dashed black line), i.e., after exhaustion of the available muscovite in A1 and B1. Figures A2, B2, A5 and B5 show the evolution of the W and Sn proportions (wt%) in minerals and melt during partial melting. Figures A3, B3, A6 and B6 show the evolution of W and Sn concentrations (ppm) in the magma during partial melting. The green and grey domains correspond to muscovite- and biotite-dehydration melting, respectively. Bi: biotite; Cd: cordierite; Grt: garnet; ilm: ilmenite; Ksp: K-feldspar; Sill: sillimanite; Mt: magnetite; Mus: muscovite; Opx: orthopyroxene; Pl: plagioclase; Qtz: quartz.

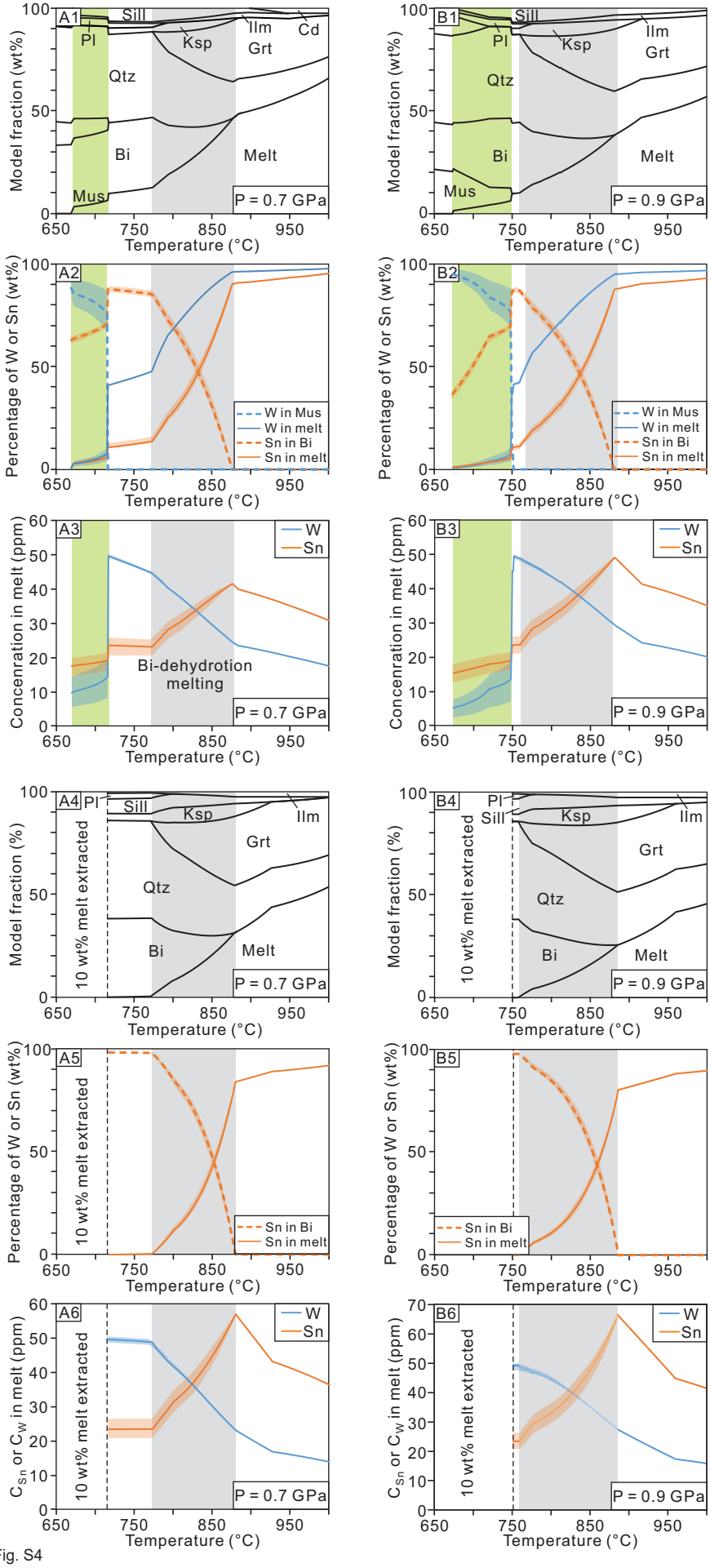
A1
Sill
Pl
Ksp
Ilm
Cd
Grt
Qtz
Bi
Melt
Mus
P = 0.7 GPa
Model fraction (wt%)
Temperature (°C)
B1
P = 0.9 GPa
A2
W in Mus
W in melt
Sn in Bi
Sn in melt
Percentage of W or Sn (wt%)
B2
A3
W
Sn
Bi-dehydrotion melting
Concenration in melt (ppm)
B3
A4
10 wt% melt extracted
Model fraction (%)
B4
A5
B5
A6
C_{Sn} or C_W in melt (ppm)
B6

Fig. S4